Beta burst coupling across the motor circuit in Parkinson's disease

Gerd Tinkhauser[a,b,c], Flavie Torrecillos[a,b], Yann Duclos[d], Huiling Tan[a,b], Alek Pogosyan[a,b], Petra Fischer[a,b], Romain Carron[e,f], Marie-Laure Welter[g,h], Carine Karachi[h,i], Wim Vandenberghe[j,k], Bart Nuttin[j,l], Tatiana Witjas[d,m], Jean Régis[e], Jean-Philippe Azulay[d,m], Alexandre Eusebio[d,m], Peter Brown[a,b,*]

[a] Medical Research Council Brain Network Dynamics Unit, University of Oxford, Oxford, UK
[b] Nuffield Department of Clinical Neurosciences, John Radcliffe Hospital, University of Oxford, Oxford, UK
[c] Department of Neurology, Bern University Hospital and University of Bern, Switzerland
[d] Institut de Neurosciences de La Timone UMR 7289, Aix Marseille Université, CNRS, 13385 Marseille, France
[e] APHM, CHU Timone, Department of Stereotactic and Functional Neurosurgery, 13385 Marseille, France
[f] Institut de Neurosciences des Systèmes UMR 1106, Aix Marseille Université, Inserm, 13385, Marseille, France
[g] CHU Rouen, Neurophysiology Department, Rouen University, 76000 Rouen, France
[h] Université Pierre et Marie Curie-Paris 6, Centre de Recherche de l'Institut du Cerveau et de la Moelle épiniere (CRICM), UMR-S975, Paris, France
[i] APHP, Groupe Hospitalier Pitié-Salpêtrière, Neurosurgery Department, 75013 Paris, France
[j] Department of Neurosciences, KU Leuven, 3000 Leuven, Belgium
[k] Department of Neurology, University Hospitals Leuven, 3000 Leuven, Belgium
[l] Department of Neurosurgery, University Hospitals Leuven, 3000 Leuven, Belgium
[m] APHM, CHU Timone, Department of Neurology and Movement Disorders, 13385, Marseille, France

ARTICLE INFO

ABSTRACT

Exaggerated activity in the beta band (13–35 Hz) is a hallmark of basal ganglia signals in patients with Parkinson's disease (PD). Beta activity however is not constantly elevated, but comes in bursts. In previous work we showed that the longer beta bursts are maintained, the more the oscillatory synchronisation within the subthalamic nucleus (STN) increases, which is posited to limit the information coding capacity of local circuits. Accordingly, a higher incidence of longer bursts correlates positively with clinical impairment, while the opposite is true for short, more physiological bursts. Here, we test the hypothesis that beta bursts not only indicate local synchronisation within the STN, but also phasic coupling across the motor network and hence entail an even greater restriction of information coding capacity in patients with PD. Local field potentials from the subthalamic nucleus and EEG over the motor cortex area were recorded in nine PD patients after temporary lead externalization after surgery for deep brain stimulation and overnight withdrawal of levodopa. Beta bursts were defined as periods exceeding the 75th percentile of signal amplitude and the coupling between bursts was considered using two distinct measurements, first the % overlapping (%OVL) as a feature of the amplitude coupling and secondly the phase synchrony index (PSI) to measure the phase coupling between regions. %OVL between STN and cortex and between the left and the right STN was higher than expected between the regions than if they had been independent. Similarly, PSI was higher during bursts as opposed to non-bursts periods. In addition, %OVL was greater for long compared to short bursts. Our results support the hypothesis that beta bursts involve long-range coupling between structures in the basal ganglia-cortical network. The impact of this is greater during long as opposed to short duration beta bursts. Accordingly, we posit that episodes of simultaneously elevated coupling across multiple structures in the basal ganglia-cortical circuit further limit information coding capacity and may have further impact upon motor impairment.

---

1. Introduction

Exaggerated beta activity in the local field potential (LFP) activity recorded in the basal ganglia is related to the motor symptoms of patients with Parkinson's disease (PD) (Kühn et al., 2006; Chen et al., 2010; Eusebio et al., 2011; Ozkurt et al., 2011; Oswal et al., 2016; Trager et al., 2016). Physiologically, beta activity appears as relatively short-lived phasic bursts in basal ganglia-cortical motor circuits (Murthy and Fetz, 1992, 1996; Kilner et al., 2003; Feingold et al., 2015). To better understand the characteristics of beta bursts in the Parkinsonian state, we previously investigated their local dynamics within the subthalamic nucleus (STN) in patients with PD (Tinkhauser et al., 2017a,b). Beta bursts in the STN of patients with PD have been shown to have a longer duration as opposed to the same patients when they are ON levodopa treatment and also compared to basal ganglia-cortical circuits in healthy non-human primates (Feingold et al., 2015; Tinkhauser et al., 2017a,b). Also important is the relationship between the duration and the amplitude of beta bursts, whereby the longer beta bursts last, the more their amplitude increases (Tinkhauser et al., 2017a,b). Increasing local field potential amplitude is thought to evidence increasing local neuronal synchronisation. As synchronised neurons are more likely to fire together, the opportunity for them to individually carry different information is diminished and the circuit's information-coding capacity ultimately restricted (Brittain and Brown, 2014). Eventually this outstrips any advantage to be had from the improvement in signal to noise ratio through neuronal synchronisation (Brittain and Brown, 2014; Fries, 2015). In line with this, we found that the higher the incidence of long beta bursts the worse the clinical impairment in PD (Tinkhauser et al., 2017a,b), and that selectively abbreviating long duration beta bursts through adaptive deep brain stimulation (aDBS) in the STN improves motor symptoms (Little et al., 2013a; Tinkhauser et al., 2017b).

However, information coding capacity may be compromised not only by excessive local synchrony but also by synchrony within the whole cortico-basal ganglia network. We have previously shown that between left and right STN the burst overlapping is greater during OFF compared to ON levodopa and the phase synchronisation greater during burst compared to non-burst periods (Tinkhauser et al., 2017b). Studies to date have not addressed whether beta bursts extend to involve cortical motor areas. Some degree of subcortico-cortical coupling might be expected considering the presence of coherent activity between the motor cortex and basal ganglia (Lalo et al., 2008; Litvak et al., 2011; Little et al., 2013b; Kato et al., 2015; Neumann et al., 2015; West et al., 2017), although these studies have not explicitly investigated the dynamic nature of any coupling. Here, we test the hypothesis that beta bursts not only indicate dynamically elevated local synchronisation within the STN, but also phasic coupling across the motor network. This then entails an even greater restriction of information coding capacity within the basal ganglia-cortical circuit in patients with PD. Coupling was considered using two distinct measurements, i.e. the % overlapping (%OVL) as a feature of the amplitude coupling and the phase synchrony index (PSI) to measure the phase coupling between regions (STN and contralateral STN as well as STN and ipsilateral motor cortex). We hypothesised that both forms of coupling would be greater during bursts than during inter burst periods, and greater for long than short duration bursts, which would further support their restrictive impact on the information coding capacity of basal ganglia-cortical circuits.

2. Methods

2.1. Subjects and surgery

We investigated the coupling of beta bursts across a motor circuit sampled with bilateral STN LFP and scalp EEG recordings in nine patients (18 hemispheres) with advanced PD undergoing STN-DBS surgery (see supplementary table). The clinical details of the patients are summarized in the supplementary material. The study was approved by the local ethics committee and all subjects gave their written informed consent. The DBS surgery was performed bilaterally with implantation of the Medtronic 3389 DBS lead (Medtronic Neurological Division) with four platinum-iridium cylindrical surfaces (1.27 mm diameter and 1.5 mm length) and a centre-to-centre separation of 2 mm as previously reported (Fluchere et al., 2014; Vercruysse et al., 2014). Proper placement of the lead was assisted by intra-operative micro-recordings (3 to 4 simultaneously passing micro-electrodes on each side), macro-stimulation during surgery and postoperative clinical improvement. The final position of the lead was confirmed or validated by fusion of preoperative MRI and postoperative CT scans (Leksell Surgiplan Version 101.1.1).

2.2. Experiments and recordings

The experimental protocol entailed the following steps: 1. DBS electrodes were temporarily externalized prior to being connected to the implantable pulse generator, the experimental session took place 3.7 days (range 3 to 6 days) after DBS surgery. 2. Patients were withdrawn from their dopaminergic medication the night before the recordings. 3. Brain signals were recorded for 2–3 min with the patient at rest, comfortably sitting in a chair and the resting state was confirmed visually. LFPs were recorded from adjacent bipolar contact pairs (01, 12, 23) to limit the impact of volume conduction from distant sources (Marmor et al., 2017). The frequency power spectrum was calculated for each bipolar channel (01, 12, 23) from the entire resting state signal. We then selected the contact pair with the highest mean beta amplitude, with the beta frequency range being defined as 13–35 Hz (see table and resting state spectral characteristics in the supplementary material). This definition of the beta frequency range is in line with previous work on beta bursts (Tinkhauser et al., 2017a,b). EEG was recorded from the scalp overlying the region of the primary motor cortex from contacts C3-Cz (left hemisphere) and C4-Cz (right hemisphere). Note, in one hemisphere the C3 EEG signal trace was not recorded, thus cortical signals were available in 17/18 hemispheres. We chose C3 and C4 as these best pick up the motor activity from motor cortex (Homan et al., 1987). Functional connectivity in the form of coherence has been previously demonstrated between these electrodes and the STN (Tan et al., 2014). Bipolar signals (C3-Cz, C4-Cz) were used so as to limit the impact of volume conduction and increase the distinction between the two hemispheres. Both LFPs and EEGs were recorded simultaneously at a sampling frequency of 2048 Hz using a TMSi-Porti (Twente Medical Systems International, Netherlands) amplifier. This is a DC amplifier with 22-bit resolution and an anti-aliasing low-pass filter of 553 Hz. All signal sources (LFP and EEG) were plugged into the same TMSi-Porti, and simultaneously recorded with a common average reference. The technical specifications of the manufacturer confirm that simultaneously recorded signals are synchronous, and this was also confirmed by the simultaneous presence of rare electrical spike artefacts across all channels (likely due to fridge motor switching). Because of this simple recording set-up, with no additional peripheral sensors and recordings made at rest, we had no major problem with artefacts in this data set. Accordingly, only very few traces demonstrated brief spike artefacts upon visual inspection and these were spliced out, using Spike2 Software (CED Cambridge Electronic design limited, United Kingdom). Then the data were imported into Matlab (version R 2015b; MathWorks, Natick, MA), for all further signal-processing analysis. Signal duration ranged from 119.2 s to 155.5 s with a mean duration of 127.2 s ± 2.5 (standard error of the mean).

2.3. Signal pre-processing

We estimated the temporal overlap and PSI between bursts at different sites (STN-cSTN, STN-iCtx). Both measures of coupling were expressed as averages of values taken across the beta band, and also as
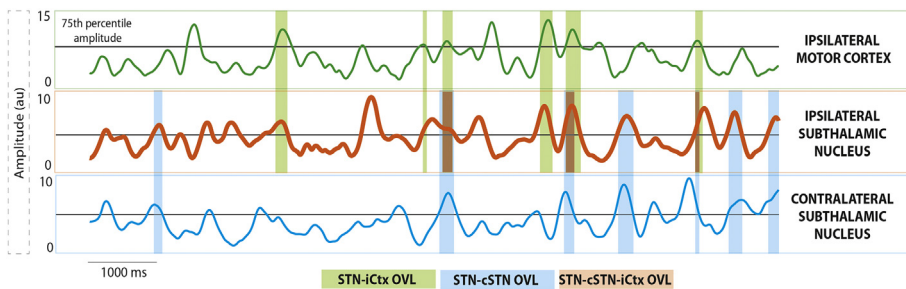
Fig. 1. Burst determination and burst overlapping: 10s segment of the 25 Hz time-evolving amplitude from the cortical EEG (green) as well as LFPs from the ipsilateral (orange) and contralateral (blue) STN. For each amplitude trace the individual 75th percentile amplitude threshold was set (back horizontal line) and periods of the signal that exceeded this threshold were defined as beta bursts (see also Methods section). Burst periods that co-occurred between pairs of signals or between all three signals were defined as overlapping burst periods. The green shaded bars indicate overlapping bursts between the ipsilateral STN and the ipsilateral motor cortex, whereas the blue shaded bars show overlapping bursts between the ipsilateral and contralateral STN. The orange shaded bar indicates burst periods occurring simultaneously in all three structures (STN-cSTN-iCtx). STN = ipsilateral subthalamic nucleus, cSTN = contralateral subthalamic nucleus; iCtx = ipsilateral motor cortex. (For interpretation of the references to colour in this figure legend, the reader is referred to the web version of this article.)

frequency varying measures plotted with 1 Hz resolution over 10–35 Hz. Bursts were defined using a default threshold consisting of 75th percentile crossing of the signal amplitude, as in previous work (Tinkhauser et al., 2017a,b), unless otherwise indicated. However, the intention was not to characterise all these burst events as biologically significant events, as applying an amplitude threshold to even a random noise signal will detect "events". Rather, our purpose was to distinguish events that might prove to present frequency-selective temporal overlapping of bursts across sites and phase synchronisation between sites higher than in non-burst periods. Here, these special characteristics related to the frequency-selective temporal overlapping of bursts across sites and phase synchronisation between sites that exceeded that expected by chance and that present in non-burst periods. Previously, we have also shown that a further characteristic is the incrementing of local burst amplitude with lengthening burst duration (Tinkhauser et al., 2017a,b).

Fig. 1 illustrates how bursts and the overlapping between bursts were determined. Both LFP and EEG signals were resampled to 200 Hz, highpass filtered at 3 Hz and decomposed into frequency components between 10 and 35 Hz with a frequency resolution of 1 Hz using a Wavelet transformation (ft_specest_wavelet script in Fieldtrip - Morlet Wavelet, width = 10, gwidth = 5; Donders Institute for Brain, Cognition and Behaviour, 2010). The burst determination algorithm was similar to the one used in our previous work (Tinkhauser et al., 2017a,b). However, instead of deriving beta bursts from the frequency of the beta peak only, we derived bursting for each frequency bin between 10 and 35 Hz. This frequency range includes both the upper and lower beta bands, which have been previously reported to have partially different characteristics (Oswal et al., 2016). We were thereby able to discern any frequency specificity within the 10–35 Hz frequency band. The time evolved wavelet amplitude from each frequency bin was smoothed (0.2 s) and all periods where the amplitude exceeded the 75th percentile were defined as bursts. We did not consider bursts with durations shorter than 2 cycles of the corresponding beta frequency (e.g. 100 ms for the 20 Hz bin) to limit the contribution of spontaneous fluctuations in amplitude due to noise.

2.4. Burst coupling measurements

The bursts were defined in their entirety ("all" bursts), and as short and long duration bursts in order to explore any pathophysiological significance of burst duration (see Supplementary Fig. 1). To this end, we sorted bursts according to their duration from short to long and calculated the cumulative burst time (Supplementary Fig. 1D). The short bursts were defined as those bursts located between the leftmost end (containing the shortest bursts) and the ½ cumulative burst time. The marginal burst that coincided with the ½ cumulative burst time was also included as a short burst. The remaining bursts were defined as long bursts. Importantly, the total burst time in the two groups was therefore approximately matched, while the number of short bursts was

consequently greater than that of the long bursts. This step was necessary to militate against the intuitive confound that longer bursts might show more overlapping because they spend more time above threshold. By matching the cumulative burst time between short and long duration bursts, the overlapping due to chance for short and long bursts should be the same, as illustrated in Supplementary Fig. 2.

2.5. Burst overlapping

The signals in each frequency bin were classified at each time-point (every 5 ms) in to whether they were part of a burst (whether short or long) and given the value 1, or part of a non-burst period and given the value 0. To calculate the burst overlapping we first added the transformed time series from the STN to those of the paired region, either the contralateral STN (cSTN) or ipsilateral cortex (iCtx) (see Fig. 1). Then the percentage duration of overlapping bursts relative to the total burst duration in the iSTN was calculated (%OVL). The expression of this measurement as a normalised value was crucial since the total burst duration between subjects varied. The same procedure was also repeated for the same regions separately for short and long bursts. Furthermore, in another sub-analysis we investigated the simultaneous burst overlapping for the short and long burst fractions across the extended motor network where all three regions (STN, cSTN and iCtx) were considered.

For all iterations where we compared the %OVL between conditions, we also calculated the %OVL due to chance by setting a variable break point in the 0 or 1 transformed burst data series and reversing and joining the two segments together. This method maintained the integrity of bursts (number and duration of bursts remained the same), but destroyed any biologically driven overlapping between bursts, leaving only that due to chance. The mean %OVL due to chance was then calculated after 100 such iterations with randomly selected break points (see illustration in Supplementary Fig. 3).

2.6. Phase synchrony index

In order to investigate the strength of phase coupling between beta bursts across circuits (iSTN-cSTN and iSTN-iCTx), the phase synchrony index was calculated for burst and non-burst periods. The way we calculated the PSI between the 2 signals is illustrated in Supplementary Fig. 4. To systematically compare the PSI across frequency bins and conditions, we first derived beta bursts in the reference signal from the ipsilateral subthalamic nucleus and then within each burst we identified the most centrally located segment of 150 ms duration. The sample points of these segments were then transformed to a phase series of the iSTN signal, together with similar transformation of the simultaneously recorded cSTN/iCtx signal over the corresponding segments. For each of the two regions a new phase time series was created by joining together the phase segments and the PSI was calculated between the two vectors (iSTN-iCtx; iSTN-cSTN). The PSI was calculated according to the

following formula, in which n is the number of time points, and φ_{iSTN} is the phase angle for the ipsilateral STN (reference signal) and $\varphi_{cSTN/iCtx}$ the phase angle for the contralateral STN or ipsilateral Ctx.

$$PSI = n^{-1} \sum_{t=1}^{n} e^{-i(\varphi_{iSTN} - \varphi_{cSTN/iCtx})}$$

The same procedure was repeated for non-burst periods, by taking the 150 ms burst-free periods that ended 50 ms before the amplitude threshold was crossed to give the next burst. Moreover, to militate against phase coupling due to spurious volume conduction, frequency bins with significant PSI differences between burst and non-burst periods were also re-assessed by calculating the PSI based on the imaginary part of the complex signal (Nolte et al., 2004). Phase coupling was not only assessed and compared between all burst and non-burst periods, but also between short and long beta bursts.

2.7. Impact of threshold

The selection of a given percentile amplitude threshold to determine bursts is somewhat arbitrary, however we have previously shown that relative differences in the two key burst parameters, burst duration and burst amplitude, are preserved across a selection of amplitude thresholds between and including the 55th to 90th percentile (Tinkhauser et al., 2017a,b). Thus a 75th percentile amplitude threshold provides a representative default option. Similarly, in this study we used a 75th percentile amplitude threshold, but also repeated key analyses (%OVL and PSI) for bursts derived by using the 50th up to the 85th percentile amplitude threshold.

2.8. Data analyses and statistics

All statistical analyses were performed in MATLAB. To evaluate statistical significance between burst parameters we first compared the average burst coupling across the beta band (13–35 Hz) (Brown, 2003) and then in more detail we tested the coupling for each single frequency bin from 10 to 35 Hz. For this we used a cluster-based permutation procedure applied to the original data: *P*-values were derived by randomly permuting the assignment of the relevant condition labels (outlined in figure labels and text) of the original data for all hemispheres 2000 times. For each frequency point the z-statistic of the actual mean difference was computed based on the distribution of the 2000 differences resulting from permutation. The resulting *P*-values were then corrected for multiple comparisons as follows: Suprathreshold clusters (pre-cluster threshold: $P < .05$) were determined for each permutation, and the sum of the z-statistics within these clusters was stored to form a distribution of the largest suprathreshold-cluster values. Finally, the 95th percentile of this distribution served as statistical threshold for the map of the actual z-statistics of the real difference (Maris and Oostenveld, 2007). Thus only those significant clusters that exceeded the threshold survived the cluster-based permutation correction. Note, for this more detailed comparison of each single frequency bin we included all those frequencies from 10 Hz up to 35 Hz that were illustrated in spectral plots.

Pairwise comparisons of the averaged beta burst coupling (%OVL, PSI) and imaginary coherence control analyses were performed using the non-parametric Wilcoxon signed-rank test. If multiple comparisons were made, *p*-values were subjected to false discovery rate (FDR)-correction, which controls the expected proportion of falsely rejected hypotheses (Benajmini and Hochberg, 1995). Results are expressed as mean values ± standard error of the mean (SEM).

3. Results

3.1. Burst overlapping between sites increases with the duration of beta bursts

The %OVL of all beta bursts over the whole beta band (13–35 Hz) for STN-ipsilateral motor cortex (iCtx) and STN-contralateral STN (cSTN) (24.26% ± 0.03 n = 17, p ≤ .001, 24.27% ± 0.03 n = 18 = 7.20, p ≤ .001, respectively), was significantly greater than the %OVL expected by chance (average: 24.26% ± 0.03 and 24.27% ± 0.03 for STN-iCtx and STN-cSTN, respectively; Supplementary fig. 5). We also compared the %OVL between short and long duration beta bursts averaged over the whole beta band (13–35 Hz) across sites. This was 13.26% ± 0.26 and 15.91% ± 0.69 for STN-iCtx and 13.30% ± 0.35 and 17.47% ± 0.63 for STN-cSTN for short and long bursts, respectively. Such overlapping could have also occurred just by chance, so we subtracted the overlapping estimated by chance in each subject and repeated the above estimation. This still confirmed greater %OVL during longer bursts compared to during shorter bursts for both sites (STN-iCtx: 4.21% ± 0.67 vs. 1.17% ± 0.26, n = 17, p = .0014 and STN-cSTN: 5.76% ± 0.63 vs. 1.18% ± 0.36, n = 18, p < .001; Fig. 2A,C). Thereafter, we independently defined burst duration with 1 Hz resolution from 10 to 35 Hz, and corrected for overlapping by chance (Fig. 2). Differences between short and long bursts were significant and centred on cluster based permutation tests around 24 Hz for both the coupling between STN-iCtx and between STN-cSTN. Importantly, since cumulative durations of short and long beta bursts were matched, and %OVL by chance was subtracted, this finding did not simply reflect that longer bursts cover more contiguous time points. The increased propensity for bursts to overlap, particularly when burst duration was longer, was also present when all the three locations were simultaneously considered, STN-cSTN-iCtx (uncorrected long vs short bursts: 3.25% ± 0.24 and 1.86% ± 0.10; long vs short bursts corrected for chance: 1.87% ± 0.24 vs. 0.39% ± 0.10, n = 17, p < .001) (Fig. 3). The % OVL between short and long duration beta bursts and their combination (all bursts) across both pairs of sites and across the triplet of recorded sites were all significantly different to chance (supplementary fig. 3). We also tested if the relative difference in %OVL between short and long bursts would persist across different burst definition thresholds and derived the % OVL for short and long beta bursts defined over a range of percentile amplitude thresholds (50th, 55th, 60th, 65th, 70th, 75th, 80th, 85th). The %OVL between bursts derived with a lower amplitude threshold was less than between those derived with a higher amplitude threshold (50th vs 85th percentile thresholds; STN-iCtx: 2.79% ± 0.37 vs. 4.44% ± 0.64, n = 17, p < .001 and STN-cSTN: 3.31% ± 0.47 vs. 5.50% ± 0.73, n = 18, p < .001; Fig. 4A, C). This was despite the substantially decreased probability of bursts derived with a higher threshold compared to those derived with lower thresholds (supplementary fig. 8). Most importantly, however, the mean ratio of % OVL of long to short duration beta bursts remained above 2.5 for the different thresholds (Fig. 4E), so that overlapping above chance was about three-fold greater during long as opposed to short beta bursts.

3.2. Phase coupling between sites is greater during bursts compared to non-burst periods

The overlapping of bursts in time across sites represents a form of amplitude co-modulation or coupling across sites. However, coupling was also evident in the phase domain, which reflects coupling with a higher temporal resolution. Fig. 5 illustrates the PSI between STN-iCtx and STN-cSTN for (duration matched) burst and non-burst periods. Here short and long bursts were combined. On average phase coupling during beta bursts was substantially greater than outside of bursts for both sites, STN-iCtx (0.20 ± 0.02 vs. 0.12 ± 0.01, n = 17, p < .001) and STN-cSTN (0.21 ± 0.02 vs. 0.12 ± 0.01, n = 18, p < .001).

% Overlap between STN-iCtx

% Overlap between STN-cSTN
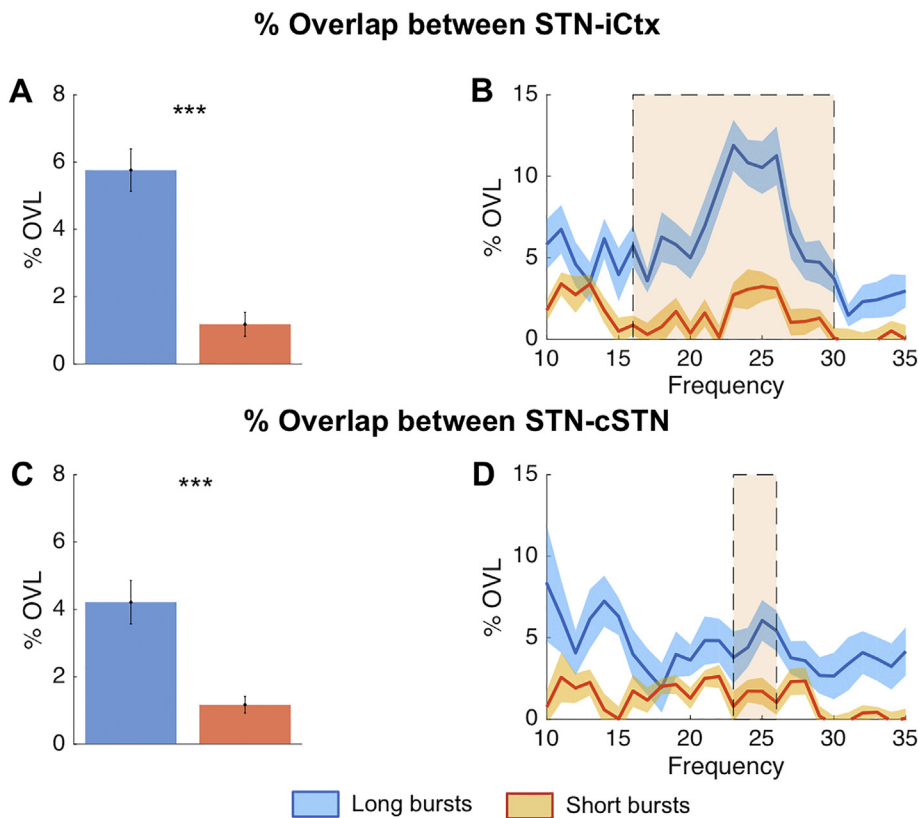
Long bursts Short bursts

Fig. 2. Burst overlapping of short and long duration beta bursts: %OVL in time for short and long bursts between STN and iCtx (A,B) and between STN and cSTN (C,D) corrected for overlapping by chance. For both pairs of sites, long duration beta bursts show on average more % overlap across beta frequency bins compared to short duration beta bursts (A: $n = 17$, $p = .0014$ and C: $n = 18$, $p < .001$, respectively). Cluster based permutation tests revealed significant differences (shaded areas) around 24 Hz for both STN-iCtx (B) and STN-cSTN (D), although the latter involved more frequency bins. Note, the cumulative burst duration between short and long duration beta bursts is matched, hence overlapping by chance is similar for each (~12%) and would not explain the greater overlapping of long duration beta bursts. To really focus on the %OVL which is beyond the % overlap expected due to chance, we subtracted this from the effective %OVL and display the %overlap corrected for chance on the y axis. Please see supplementary fig. 1 for how short and long duration beta bursts were defined. Values presented as mean ± SEM. *** $p < .001$; STN = ipsilateral subthalamic nucleus, cSTN = contralateral subthalamic nucleus; iCtx = ipsilateral motor cortex.

Across frequencies the PSI difference was frequency selective and significant on cluster based permutation tests between 13 and 16 Hz and 18–27 Hz, and between 10 and 17 Hz and 24–31 Hz for the comparison between STN-iCtx and STN-cSTN, respectively. To further militate against spurious volume conduction as a driver of PSI differences, we calculated the PSI based only on the imaginary part of the complex signal over these frequency bands. This too was significantly different between burst and non-burst periods for both STN-iCtx ($n = 17$, $p < .001$) and STN-cSTN ($n = 18$, $p < .001$) (Fig. 5E-F).

3.3. Phase coupling differences between long and short bursts were small

In addition, we confirmed that, in line with Fig. 5, short and long bursts showed stronger phase coupling compared to non-burst periods for STN-iCtx and STN-cSTN (supplementary fig. 6). As beta frequency band amplitude co-modulation between sites increased during longer

bursts we determined whether coupling in the phase domain might similarly increase in long as opposed to short beta bursts. However, no significant difference was found between the PSI of longer bursts and that of shorter bursts (supplementary fig. 7A, C; STN-iCtx 0.25 ± 0.02 vs. 0.23 ± 0.02, $n = 17$, $p = .07$ and STN-cSTN 0.25 ± 0.01 vs. 0.24 ± 0.01, $n = 18$, $p = .07$), nor when comparing all individual frequencies (supplementary fig. 7B, D). Moreover, the similarity in PSI between short and long bursts was a maintained feature across different amplitude thresholds (Fig. 4B, D), and the ratio between the PSI of short and long duration beta bursts approximated unity (Fig. 4F).

4. Discussion

Our study investigates the temporal relationship between beta bursts across the basal ganglia-cortical network in patients with Parkinson's disease. We applied two measures that emphasise temporal

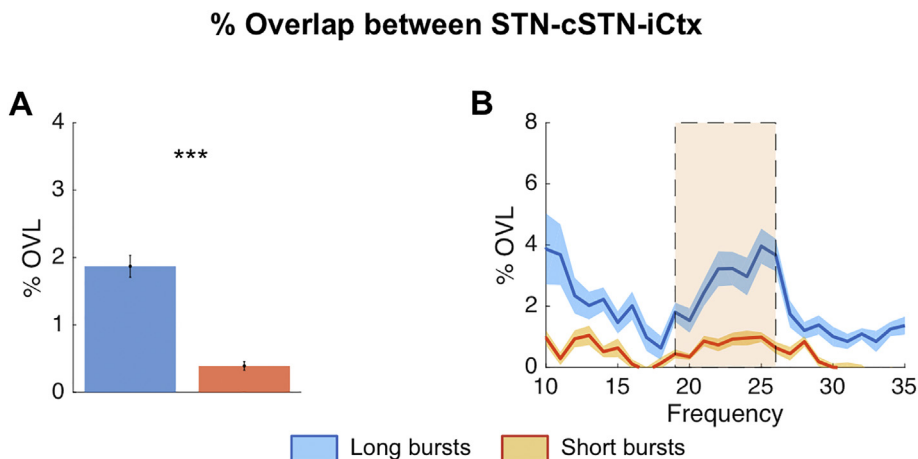## % Overlap between STN-cSTN-iCtx

Long bursts Short bursts

Fig. 3. Burst overlapping across the extended motor network: % simultaneous overlap for short and long beta bursts between all three regions: STN-cSTN-iCtx (triple overlapping). Long duration beta bursts show an overall greater average %OVL compared to short beta bursts across this extended motor network (A: $n = 17$, $p < .001$), with a significant (shaded area) between 19 and 26 Hz (B). Note, overlapping by chance has already been subtracted. Values presented as mean ± SEM. *** $p < .001$; STN = ipsilateral subthalamic nucleus, cSTN = contralateral subthalamic nucleus; iCtx = ipsilateral motor cortex.

Coupling STN-iCtx

A

B

Coupling STN-cSTN

C

D

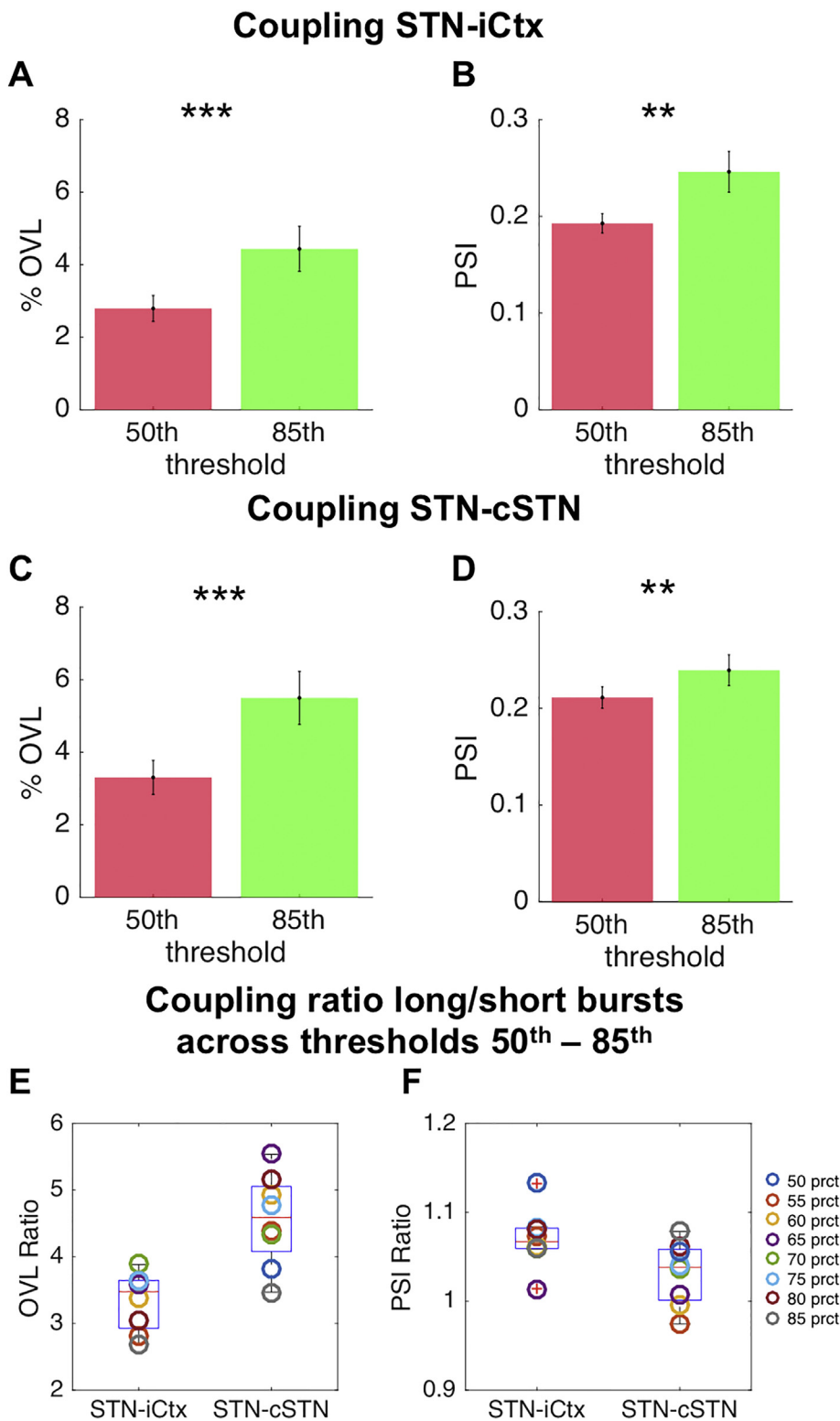## Coupling ratio long/short bursts across thresholds 50th − 85th

E

F

Fig. 4. Impact of amplitude threshold on %OVL and PSI: Illustrates the %OVL and PSI for beta bursts derived with a 50th (red) and 85th (green) percentile amplitude threshold for both pairs of sites (A,B: STN-iCtx; C,D: STN-cSTN). The %OVL (A and C, both corrected for the threshold specific overlapping by chance) is significantly greater for bursts derived with the 85th percentile amplitude threshold compared to those derived with the 50th percentile amplitude threshold (STN-iCtx: $n = 17$, $p < .001$; STN-cSTN: $n = 18$, p < .001). This is despite the reduced burst probability when a higher percentile threshold was used (supplementary fig. 8). Similarly, the PSI (B and D) for bursts derived with the 85th percentile amplitude threshold was greater than that derived with the lower amplitude threshold (STN-iCtx: n = 17, $p = .009$; STN-cSTN: n = 18, p = .009). The coupling ratios between long and short beta bursts derived from a selection of percentile amplitude thresholds (50th, 55th, 60th, 65th, 70th, 75th, 80th, 85th) are illustrated in E (Ratio OVL) and F (Ratio PSI). The positive median coupling ratios demonstrated in the box and whisker plots confirm that the stronger coupling in long as opposed to short beta bursts is preserved across different thresholds. Values presented as mean ± SEM. * $p < .05$, ** $p < .01$, *** $p < .001$; STN = ipsilateral subthalamic nucleus, cSTN = contralateral subthalamic nucleus; iCtx = ipsilateral motor cortex. (For interpretation of the references to colour in this figure legend, the reader is referred to the web version of this article.)

coupling on different scales: first the % burst overlapping between bursts to reveal the relationship between interregional beta bursts over hundreds of milliseconds, and second, phase synchronisation to assess the coupling between individual and successive beta cycles over shorter time periods. We have previously shown that between left and right STN the burst overlapping is greater during OFF compared to ON levodopa and the phase synchronisation greater during burst compared to non-burst periods (Tinkhauser et al., 2017b). Here we confirm these findings in a different patient cohort, extend them to the coupling between STN and cortex, and demonstrate that the temporal overlapping between bursts at different sites increases still further during long bursts. In this regard overlapping followed the same general pattern as LFP amplitude in the STN which increases with burst duration (Tinkhauser et al., 2017a,b). In contrast, phase synchronisation between sites was established early on in beta bursts, and did not significantly increase if bursts became prolonged. That said, any impact of
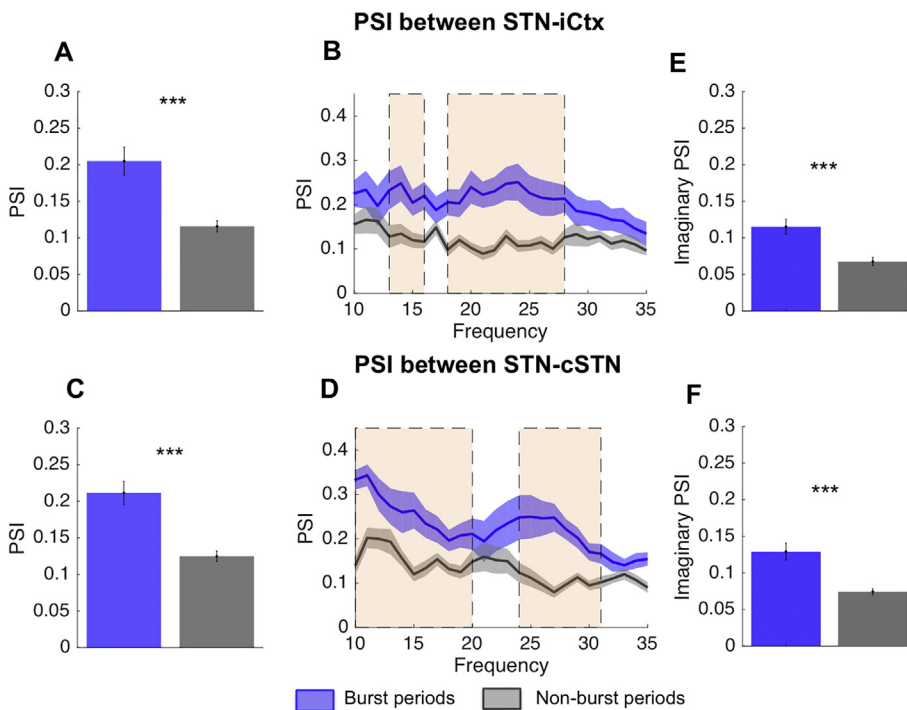
Fig. 5. Phase synchrony index during and between bursts: PSI for burst periods (blue) and non-burst periods (grey) between STN and iCtx (A,B) and between STN and cSTN (C,D). Bursts defined using a 75th percentile amplitude threshold. For both pairs of sites, bursts show on average a greater PSI compared to non-burst periods (A: n = 17, p < .001 and C: n = 18, p < .001). In cluster-based permutation tests this proved significant (shaded areas) around 13–16 Hz and 18–27 Hz between STN and motor Ctx (A) and between 10 and 20 Hz and 24–31 Hz for the comparison between STN and cSTN (D). Over the frequency range of the significant clusters, phase locking was recalculated using the imaginary part of the signal (E, F) and differences remained significant for both comparisons (STN-iCtx n = 17, p < .001) and STN-cSTN n = 18, p < .001). Hence phase locking differences could not be simply ascribed to variations in volume conduction. Values presented as mean ± SEM. *** p < .001; STN = ipsilateral subthalamic nucleus, cSTN = contralateral subthalamic nucleus; iCtx = ipsilateral motor cortex. (For interpretation of the references to colour in this figure legend, the reader is referred to the web version of this article.)

phase synchronisation between sites will still be greater during long bursts, by virtue of the fact that it is sustained for longer. In sum, our results suggest that interregional coupling at beta frequencies between motor cortex and basal ganglia is not a constant phenomenon, but is concentrated into bursts. This becomes particularly important when we consider novel treatment strategies such as closed loop DBS (Little et al., 2013a) where recent evidence suggests that long duration beta bursts should be preferentially terminated (Tinkhauser et al., 2017b). The current work supports this view in so far as long duration beta bursts are shown to involve not only local synchronisation, but also pathological synchronisation across the motor network.

Why might the coupling between sites in the basal ganglia-cortical circuit evident in bursts be important? One reason might be that within a complex looped architecture like the basal ganglia-motor circuit there may be degeneracy, at least in the face of some task demands, and the potential for compensation. Here we use the term degeneracy to describe the ability of elements that are structurally different to perform the same function (Tononi et al., 1999). Degeneracy and compensation place limits on the functional impact of focal lesions, and for these reasons multiple and distributed lesions that outstrip degeneracy and obviate compensation may have much more devastating impacts. The functional effect of pathologically elevated beta band synchrony has been considered akin to that of a reversible information lesion due to the mutual information shared by synchronous events (Mallet et al., 2008; Hanslmayr et al., 2012; Brittain and Brown, 2014), and there is little reason to suspect that the impact of temporary local information lesions will not be similarly governed by degeneracy and any potential for, in this case acute, compensation. An example of this can be seen in epilepsy, where the short-lived but progressive recruitment of more than one connected site may lead to clinically-evident seizure activity (Lounasmaa et al., 1996). Accordingly, we posit that episodes of simultaneously elevated synchronisation at multiple nodes in the basal ganglia-cortical circuit, and of their phase coupling, will have much greater impact upon function than isolated bursts of local synchronisation. Yet it should be stressed that although we frame the significance of coupling within and between beta bursts in terms of the effect on the information coding capacity of the basal ganglia-cortical circuit at a given moment in time, we provide no direct measure of information

coding capacity so that this hypothesis remains presumptive. It should also be noted that we focus on the effects of pathologically elevated synchrony as reflected in high amplitude, long duration beta bursts and acknowledge that the improvement in signal to noise ratios seen with weaker levels of synchronisation may, under physiological circumstances, outweigh any limitation on information coding capacity (Brittain and Brown, 2014).

We should also consider if burst-related inter-site coupling is sufficient to temporarily limit information coding capacity. The temporal overlapping of bursts occurred almost 30% of the total burst time. Although much, but not all, of this overlapping could be expected by chance given the duration of beta bursts at different sites, this too might be expected to compromise the circuit's information coding capacity for the reasons discussed above. Instead, the importance of the significant corrected overlapping lies in the fact that it was greater during long than short beta bursts, revealing a synchronising force across the network driving additional amplitude correlation, particularly when burst duration is prolonged. One candidate mechanism for this is the progressive entrainment of oscillations that may occur when activity at one node of the network is near the resonance frequency of another site in the same network (Weinrich et al., 2017). Consistent with this we observed greater phase synchronisation during bursts than during non-burst periods. Yet, although the degree of corrected overlapping grew with increasing burst duration, phase synchronisation did not. The simplest explanation for this behaviour is that phase synchronisation rapidly reached its ceiling. However, the finding would also be compatible with a model in which the synchronisation of selected neural elements between distant sites indexed by the PSI takes time to be propagated locally to account for the increase in LFP amplitude that occurs as bursts are sustained over time. Such local synchronisation might include the recruitment of neural elements that were previously not represented in the LFP or EEG, and therefore did not affect the PSI estimation. These could be the activation of previously silent neurons or the recruitment of previously asynchronously active neurons into the beta oscillation. Asynchronously active neurons would fail to summate their activities and would contribute little to the LFP or EEG. These possibilities remain to be tested by additional multiple, high resolution recordings within the local network. The progressive increase in STN

LFP amplitude may, in fact, reflect sequences of neural entrainment originating upstream to the STN, given there is little evidence of lateral connectivity within the STN (Carpenter and Strominger, 1967; Carpenter et al., 1981),

As we focused on measures of coupling between sites it is important to consider the extent to which our results might have been confounded by volume conduction. To militate against this we used only bipolar electrodes, and, at least when derived from adjacent contacts of a DBS electrode, this has proven successful in greatly suppressing contributions from volume conduction from distant sources like the cerebral cortex (Marmor et al., 2017). Furthermore, we validated our findings with an analysis of the PSI based on the imaginary part of the complex signal guarding against the effects of volume conduction (Nolte et al., 2004). One of the advantages of our analysis pipeline was the ability to determine the precise frequency ranges of coupling measures in the beta frequency region. This resolution was motivated by the increasing evidence that there may be two relatively functionally distinct oscillatory activities in the beta band in basal ganglia-cortical networks, − one centered at around 15 Hz and one around 25 Hz (Litvak et al., 2011; van Wijk et al., 2016). Interestingly, in this cohort, if the various burst coupling results across the beta frequencies (both %OVL and PSI) were normalised and joined together, then the coupling within the beta range seemed to be greatest around 25 Hz and less pronounced, although still present, around 15 Hz (Supplementary Fig. 9). One possible explanation, is that there are two cortico-subcortical subcircuits with distinct preferred frequencies which are both susceptible to episodes of ex-aggerated coupling between nodes, although previous work has suggested that the lower frequency subcircuit is rather more likely to display pathological local, as opposed to cross-site, synchrony (van Wijk et al., 2016).

4.1. Study limitations

Recordings took place in patients with temporarily externalized leads in the immediate post-operative state. A confounding stun effect cannot therefore be excluded, leading to an underestimation of coupling (Chen et al., 2006). Furthermore, the burst distribution from short to long bursts corresponds to a continuum, and our dichotomized representation of bursts, although reasonable from a methodological point of view, has a rather arbitrary character. Similarly, other methods could be used to derive the overlapping due to chance. Moreover, further work is necessary to better characterise the possible distinction between physiological and pathological bursting and how this distinction might vary according to behavioural context. In this study we focused solely on the coupling of bursts derived from the beta frequency band defined as 13 to 35 Hz, and burst coupling across regions in other frequency bands remains to be investigated. Also, in this study no clinical assessments of the motor symptoms were made during the recording. Thus further studies are warranted to directly confirm the hypothesis that clinical impairment is greater with bursts that involve coupling across the basal ganglia cortical circuit than with bursts that are isolated at one site in this circuit.

5. Conclusion

Here we provide evidence that pathologically long beta bursts in patients with Parkinson's disease do not only involve local synchronisation within the basal ganglia-cortical circuit but also dynamic long range synchronisation in terms of amplitude correlation and phase synchrony. These attributes are less marked in shorter, perhaps more physiological, beta bursts, although still greater than outside of beta bursts. Together with the evidence that local synchrony increases as burst duration is maintained (Tinkhauser et al., 2017a,b), the current results suggest a parallel cumulative involvement in other network nodes, increasing the potential impact of beta bursts upon the information coding capacity of the system, and thereby potentially on motor performance.

Appendix A. Supplementary data

Supplementary data to this article can be found online at https://doi.org/10.1016/j.nbd.2018.06.007.

References

Benajmini, Y., Hochberg, Y., 1995. Controlling the False Discovery Rate: A Practical and Powerful Approach to Multiple Testing Author (s): Yoav Benjamini and Yosef Hochberg Source. Journal of the Royal Statistical Society. Series B (Methodological) 57, 289–300 No. 1 Published by : J R Stat. Soc B.

Brittain, J.S., Brown, P., 2014. Oscillations and the basal ganglia: motor control and beyond. NeuroImage 85, 637–647.

Brown, P., 2003. Oscillatory nature of human basal ganglia activity: relationship to the pathophysiology of Parkinson's disease. Mov. Disord. 18, 357–363.

Carpenter, M.B., Strominger, N.L., 1967. Efferent fibers of the subthalamic nucleus in the monkey. A comparison of the efferent projections of the subthalamic nucleus, substantia nigra and globus pallidus. Am. J. Anatolia 121, 41–72.

Carpenter, M.B., Carleton, S.C., Keller, J.T., Conte, P., 1981. Connections of the subthalamic nucleus in the monkey. Brain Res. 224, 1–29.

Chen, C.C., Pogosyan, A., Zrinzo, L.U., Tisch, S., Limousin, P., Ashkan, K., et al., 2006. Intra-operative recordings of local field potentials can help localize the subthalamic nucleus in Parkinson's disease surgery. Exp. Neurol. 198, 214–221.

Chen, C.C., Hsu, Y.T., Chan, H.L., Chiou, S.M., Tu, P.H., Lee, S.T., et al., 2010. Complexity of subthalamic 13-35 Hz oscillatory activity directly correlates with clinical impairment in patients with Parkinson's disease. Exp. Neurol. 224, 234–240.

Eusebio, A., Thevathasan, W., Doyle Gaynor, L., Pogosyan, A., Bye, E., Foltynie, T., et al., 2011. Deep brain stimulation can suppress pathological synchronisation in parkinsonian patients. J. Neurol. Neurosurg. Psychiatry 82, 569–573.

Feingold, J., Gibson, D.J., DePasquale, B., Graybiel, A.M., 2015. Bursts of beta oscillation differentiate postperformance activity in the striatum and motor cortex of monkeys performing movement tasks. Proc. Natl. Acad. Sci. U. S. A. 112, 13687–13692.

Fluchere, F., Witjas, T., Eusebio, A., Bruder, N., Giorgi, R., Leveque, M., et al., 2014. Controlled general anaesthesia for subthalamic nucleus stimulation in Parkinson's disease. J. Neurol. Neurosurg. Psychiatry 85, 1167–1173.

Fries, P., 2015. Rhythms for cognition: communication through coherence. Neuron 88, 220–235.

Hanslmayr, S., Staudigl, T., Fellner, M.-C., 2012. Oscillatory power decreases and long-term memory: the information via desynchronization hypothesis. Front. Hum. Neurosci. 6, 1–12.

Homan, R.W., Herman, J., Purdy, P., 1987. Cerebral location of international 10-20 system electrode placement. Electroencephalogr. Clin. Neurophysiol. 66, 376–382.

Kato, K., Yokochi, F., Taniguchi, M., Okiyama, R., Kawasaki, T., Kimura, K., et al., 2015. Bilateral coherence between motor cortices and subthalamic nuclei in patients with Parkinson's disease. Clin. Neurophysiol. 126, 1941–1950.

Kilner, J.M., Salenius, S., Baker, S.N., Jackson, A., Hari, R., Lemon, R.N., 2003. Task-dependent modulations of cortical oscillatory activity in human subjects during a bimanual precision grip task. NeuroImage 18, 67–73.

Kühn, A.A., Kupsch, A., Schneider, G.H., Brown, P., 2006. Reduction in subthalamic 8-35 Hz oscillatory activity correlates with clinical improvement in Parkinson's disease. Eur. J. Neurosci. 23, 1956–1960.

Lalo, E., Thobois, S., Sharott, A., Polo, G., Mertens, P., Pogosyan, A., et al., 2008. Patterns of bidirectional communication between cortex and basal ganglia during movement in patients with Parkinson disease. J. Neurosci. 28, 3008–3016.

Little, S., Pogosyan, A., Neal, S., Zavala, B., Zrinzo, L., Hariz, M., et al., 2013a. Adaptive deep brain stimulation in advanced Parkinson disease. Ann. Neurol. 449–457.

Little, S., Tan, H., Anzak, A., Pogosyan, A., Kuhn, A., Brown, P., 2013b. Bilateral functional connectivity of the basal ganglia in patients with Parkinson's disease and its modulation by dopaminergic treatment. PLoS One 8, e82762.

Litvak, V., Jha, A., Eusebio, A., Oostenveld, R., Foltynie, T., Limousin, P., et al., 2011. Resting oscillatory cortico-subthalamic connectivity in patients with Parkinson's disease. Brain 134, 359–374.

Lounasmaa, O., Hämäläinen, M., Hari, R., Salmelin, R., 1996. Information processing in the human brain: magnetoencephalographic approach. Proc. Natl. Acad. Sci. U. S. A. 93, 8809–8815.

Mallet, N., Pogosyan, A., Marton, L.F., Bolam, J.P., Brown, P., Magill, P.J., 2008. Parkinsonian Beta oscillations in the external Globus pallidus and their relationship

with subthalamic nucleus activity. J. Neurosci. 28, 14245–14258.

Maris, E., Oostenveld, R., 2007. Nonparametric statistical testing of EEG- and MEG-data. J. Neurosci. Methods 164, 177–190.

Marmor, O., Valsky, D., Joshua, M., Bick, A.S., Arkadir, D., Tamir, I., et al., 2017. Local vs. volume conductance activity of field potentials in the human subthalamic nucleus. J. Neurophysiology 117, 2140–2151.

Murthy, V.N., Fetz, E.E., 1992. Coherent 25- to 35-Hz oscillations in the sensorimotor cortex of awake behaving monkeys. Proc. Natl. Acad. Sci. U. S. A. 89, 5670–5674.

Murthy, V.N., Fetz, E.E., 1996. Oscillatory activity in sensorimotor cortex of awake monkeys: synchronization of local field potentials and relation to behavior. J. Neurophysiol. 76, 3949–3967.

Neumann, W., Jha, A., Bock, A., Huebl, J., Horn, A., Schneider, G., et al., 2015. Cortico-Pallidal Oscillatory Connectivity in Patients with dystonia. pp. 1894–1906.

Nolte, G., Holroyd, T., Carver, F., Coppola, R., Hallett, M., 2004. Localizing brain interactions from rhythmic EEG/MEG data. Conf. Proc. IEEE Eng. Med. Biol. Soc. 2, 998–1001.

Oswal, A., Beudel, M., Zrinzo, L., Limousin, P., Hariz, M., Foltynie, T., et al., 2016. Deep brain stimulation modulates synchrony within spatially and spectrally distinct resting state networks in Parkinson's disease. Brain 139, 1482–1496.

Ozkurt, T.E., Butz, M., Homburger, M., Elben, S., Vesper, J., Wojtecki, L., et al., 2011. High frequency oscillations in the subthalamic nucleus: a neurophysiological marker of the motor state in Parkinson's disease. Exp. Neurol. 229, 324–331.

Tan, H., Zavala, B., Pogosyan, A., Ashkan, K., Zrinzo, L., Foltynie, T., et al., 2014. Human subthalamic nucleus in movement error detection and its evaluation during Visuomotor adaptation. J. Neurosci. 34, 16744–16754.

Tinkhauser, G., Pogosyan, A., Little, S., Beudel, M., Herz, D.M., Tan, H., et al., 2017a. The modulatory effect of adaptive deep brain stimulation on beta bursts in Parkinson's disease. Brain 140, 1053–1067.

Tinkhauser, G., Pogosyan, A., Tan, H., Herz, D.M., Kühn, A.A., Brown, P., 2017b. Beta burst dynamics in Parkinson's disease OFF and ON dopaminergic medication. Brain 140, 2968–2981.

Tononi, G., Sporns, O., Edelman, G.M., 1999. Measures of degeneracy and redundancy in biological networks. Proc. Natl. Acad. Sci. 96, 3257–3262.

Trager, M.H., Koop, M.M., Velisar, A., Blumenfeld, Z., Nikolau, J.S., Quinn, E.J., et al., 2016. Subthalamic beta oscillations are attenuated after withdrawal of chronic high frequency neurostimulation in Parkinson's disease. Neurobiol. Dis. 96, 22–30.

van Wijk, B.C.M., Beudel, M., Jha, A., Oswal, A., Foltynie, T., Hariz, M.I., et al., 2016. Subthalamic nucleus phase-amplitude coupling correlates with motor impairment in Parkinson's disease. Clin. Neurophysiol. 127, 2010–2019.

Vercruysse, S., Vandenberghe, W., Munks, L., Nuttin, B., Devos, H., Nieuwboer, A., 2014. Effects of deep brain stimulation of the subthalamic nucleus on freezing of gait in Parkinson's disease: a prospective controlled study. J. Neurol. Neurosurg. Psychiatry 85, 871–877.

Weinrich, C.A., Brittain, J.S., Nowak, M., Salimi-Khorshidi, R., Brown, P., Stagg, C.J., 2017. Modulation of long-range connectivity patterns via frequency-specific stimulation of human cortex. Curr. Biol. 27 3061–3068.e3.

West, T.O., Berthouze, L., Halliday, D.M., Litvak, V., Sharott, A., Magill, P.J., et al., 2017. Propagation of Beta/Gamma Rhythms in the Cortico-Basal Ganglia Circuits of the Parkinsonian Rat.